03,09,12

# Exciton states in narrow quantum wells $In_xGa_{1-x}As/GaAs$

© N.R. Grigorieva[1], A.V. Mikhailov[2], E.S. Khramtsov[2], I.V. Ignatiev[2]

[1] St. Petersburg State University,
St. Petersburg, Russia
[2] Uraltsev Laboratory of Spin Optics, Saint-Petersburg State University
St. Petersburg, Russia

E-mail: n.r.grigorieva@spbu.ru

*Received September 12, 2023*
*Revised September 12, 2023*
*Accepted September 13, 2023*

The reflection spectra of a high-quality heterostructure with a narrow quantum well $In_xGa_{1-x}As/GaAs$ ($x = 0.022$) are studied. Microscopic modeling of the exciton spectrum is performed using a numerical solution of the three-dimensional Schrodinger equation. It is shown that two exciton resonances below the free exciton energy in GaAs are formed by a heavy hole exciton localized in a quantum well. The potential profile of a quantum well is determined within the framework of a theoretical model with parameters calculated ab initio. For the studied structure, the ratio of the discontinuities of the valence band ($E_v$) and the conduction band ($E_c$) is obtained: $E_c : E_v = 64 : 36$.

**Keywords:** excitons, polaritons, heterostructures, quantum well, microscopic calculation.

DOI: 10.61011/PSS.2023.11.57314.201

## 1. Introduction

$In_xGa_{1-x}As/GaAs$ strained structures are widely used to create highly efficient optical devices, such as LEDs and semiconductor lasers [1–3], modulators and switches [4,5]. $In_xGa_{1-x}As/GaAs$ narrow quantum wells (less than 15 nm in width) are an important part of polariton microcavities and polariton logic elements an important part of polariton microcavities and polariton logic elements [6–9].

The electronic properties of devices based on semiconductor heterostructures significantly depend on the potential profile of the quantum well (QW), in particular, on the magnitude of the band discontinuity of the barrier and QW materials. The absolute position of band extrema in unstrained semiconductor materials that make up the heterostructure can change significantly under the effect of deformation potentials [10–14].

There are various approaches to describing changes in heterojunction parameters under the effect of deformation potentials, including both theoretical calculations ab initio and using parameters obtained from experimental data [10–14]. Deformation potentials and elastic constants depend on the mechanical properties of the material and, therefore, are sensitive to both the geometry of the heterostructure and its quality, determined by the growth technology. Therefore, a unified approach to determining the values of band discontinuities in strained heterostructures has not yet been developed. The magnitude of the conduction band and valence band discontinuities for $In_xGa_{1-x}As/GaAs$ heterostructures is also the subject of research. The range of values of the material parameters of the medium varies over a fairly wide range for different solid solution concentrations, QW and barrier widths. One of the most precise methods for studying the electronic properties of semiconductor nanostructures is the method of exciton spectroscopy [14–16]. The use of this method is especially relevant in the light of the design and creation of polariton devices.

To achieve the required values of the quality factor of the microcavity, which is the main structural element of a polariton device, a high quality of the semiconductor structure is required. Therefore, the concentration range of the $In_xGa_{1-x}As$ solid solution used in the $In_xGa_{1-x}As/GaAs$ pair is often limited to a few percent to reduce the generation of defects under the effect of stresses due to the mismatch of lattice constants of $In_xGa_{1-x}As$ and GaAs. At low indium concentrations, the carrier quantization potential in a narrow QW can be comparable to the exciton binding energy, which makes it difficult to use simple models for analyzing the exciton spectrum of such structures.

In structures with narrow QWs, the depth of penetration of the exciton wave function into the subbarrier region is quite large. One of the advantages of $In_xGa_{1-x}As/GaAs$ structures with narrow quantum wells is the fact that the barriers are formed by gallium arsenide, so the exciton interacts predominantly with the crystal lattice of a binary compound with a small number of defects. However, this creates an additional difficulty when analyzing the exciton spectra of $In_xGa_{1-x}As/GaAs$ heterostructures, because hole tunneling into barriers significantly affects the effective masses of light and heavy holes, which are responsible for the exciton binding energy in narrow QWs [17–21].

In this study, the exciton reflection spectrum of a $In_xGa_{1-x}As/GaAs$ strained heterostructure with a QW with a low indium content, surrounded by wide barriers, is studied. The nature of the exciton spectrum near free exciton energy in GaAs is analyzed. Using the method of microscopic modeling, the contribution of excitonic

resonances localized in the QW was identified and their parameters were determined. Within the framework of the chosen model, the parameters of the localizing potential are determined.

Exciton reflection spectra were recorded at $T = 8\,\mathrm{K}$ according to the standard scheme at normal light incidence in the region of excitonic resonances of gallium arsenide and a narrow QW.

The sample was grown by molecular beam epitaxy (MBE) on a GaAs substrate with (001) orientation at $T = 520^\circ\mathrm{C}$. The P552 structure contains a narrow ($L^{QW1} = 2\,\mathrm{nm}$) and a wide ($L^{QW2} = 100\,\mathrm{nm}$) QWs. Nominal parameters of the heterostructure layers are: substrate GaAs:Si, buffer layer GaAs — 1100 nm ($L^{BfL}$), QW $In_xGa_{1-x}As$ ($x = 0.02-0.025$) — 2 nm, barrier layer GaAs — 130 nm ($L^{BrL}$), QW $In_xGa_{1-x}As$ ($x = 0.02-0.025$) — 100 nm, cap layer GaAs — 70 nm ($L^{CL}$).

## 2. Exciton reflectance spectra

In the reflectance spectrum, below the line of the free exciton ground state in gallium arsenide (1515 meV), 2 narrow resonances, $X1$ and $X2$, are observed, see Figure 1. Above the energy of 1515 meV, 3 narrow features, $X3$, $X4$ and $X5$, with significant amplitude can be distinguished.

To determine the parameters of exciton resonances, the reflectance spectrum was analyzed within the framework of the model of the nonlocal dielectric response of isolated exciton resonances [22]. According to the model, the reflectance coefficient is given by the following formula:

$$R(\omega) = \left| \frac{r_s(\omega) + \sum\limits_j r_{xj}(\omega)\exp(2i\varphi_j)}{1 + r_s(\omega)\sum\limits_j r_{xj}(\omega)\exp(2i\varphi_j)} \right|^2, \qquad (1)$$

where $r_s(\omega)$ is Fresnel reflectance from the heterostructure boundary; $\varphi_j$ is phase shift of the electromagnetic wave

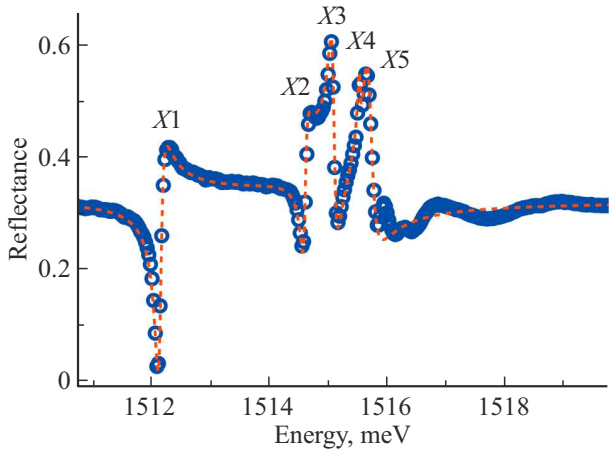


**Figure 1.** Experimental reflectance spectrum of P552 sample (circles). Model reflectance spectrum calculated using expression (1) and parameter values given in Table 1 (dashed line).

**Table 1.** Parameters of exciton resonances for model calculation using expression (1)

| Resonance | $X1$ | $X2$ | $X3$ | $X4$ | $X5$ |
|---|---|---|---|---|---|
| $\hbar\omega_0$, meV | 1512.17 | 1514.62 | 1515.09 | 1515.59 | 1515.69 |
| $\hbar\Gamma_0$, $\mu$eV | 51 | 18 | 27 | 3.6 | 41 |
| $\hbar\Gamma_{NR}$, $\mu$eV | 38 | 40 | 30 | 21 | 55 |
| $\varphi$, rad | 3.73 | 4.09 | 1.40 | 0.73 | 1.01 |

reflected from the QW located at a certain distance from the surface of the heterostructure; $r_{Xj}$ is amplitude reflectance of an isolated exciton resonance. It is given by the following formula:

$$r_{Xj}(\omega) = \frac{i\Gamma_0}{(\omega_0 - \omega) - i(\Gamma_0 + \Gamma_{NR})},$$

where $\omega_0$ is exciton resonance frequency $\Gamma_0$ is radiative decay rate, $\Gamma_{NR}$ is non-radiative decay rate.

Resonant frequencies, radiative and non-radiative decay rate, as well as phases of exciton resonances, which provide the best description of features in the range from 1512 to 1516 meV, are given in Table 1. It should be noted that the excited excitonic states $X2-X5$ are located quite close to each other, so that the energy gaps between them are comparable to the radiation broadening of resonances. In this case, to more accurately determine the parameters of these excitonic states, it is necessary to use the generalized theory described in [23–26]. This theory, however, requires complex theoretical modeling, therefore we restrict ourselves here to a simple analysis based on formulae (1) and (2). At the same time, we will keep in mind that the parameters given in Table 1 for these states have approximate values.

## 3. Microscopic model. The Hamiltonian

In order to highlight the contribution of the narrow QW and clarify the nature of the observed lines, microscopic modeling of the spectrum of excitonic states of a heterostructure with a narrow QW surrounded by wide barriers was carried out. During the modeling, positions of exciton resonances, the magnitude of radiation broadening, and the exciton binding energy were determined. Within the framework of the microscopic model for an isolated exciton state, the behavior of an exciton in a QW can be described by the following Hamiltonian [16,22]:

$$H_{diag} = \frac{k_e^2}{2m_e} + \frac{(k_{hx}^2 + k_{hy}^2)}{2m_{xy}} + \frac{k_{hz}^2}{2m_{hz}} - \frac{e^2}{\varepsilon|r_e - r_h|} + V_e(r_e) + V_h(r_h),$$

where $V_e(r_e)$ describes the profile of the conduction band potential in the QW, $V_h(r_h)$ is profile of the valence band potential in the QW, $m_{xy}$ is effective hole mass in

the QW plane; $m_{hz}$ is effective hole mass in the direction perpendicular to the QW plane; $\varepsilon$ is dielectric constant. The specific type and parameters of the electron potential $V_e(r_e)$ and hole potential $V_h(r_h)$ are determined by the growth conditions of the layer of $In_xGa_{1-x}As$ ($x = 0.02-0.025$) solid solution.

The part of the exciton wave function independent of spin variables can be represented in the following form [16,22]:

$$\psi(x, y, z_e, z_h) = \varphi(z_e, z_h, \rho)\exp(ik_\phi\phi),$$

where $x = x_h - x_e$; $y = y_h - y_e$; $\rho$, and $\phi$ are cylindrical coordinates describing the relative motion of the electron and hole in the QW plane. In turn, $\varphi(z_e, z_h, \rho)$ is determined by the parameters and profile of the QW potential [22]. In the limit of wide QWs, terms can be distinguished that describe the motion of the center of mass of the exciton along $z$ axis and the relative motion of the electron and hole due to the Coulomb interaction

$$\varphi(z_e, z_h, \rho) = F(Z)\exp(-r/a_B)/\sqrt{\pi a_B^3},$$

where $a_B$ is Bohr radius of the exciton. For narrow QWs with infinite walls, the $\varphi(z_e, z_h, \rho)$ function tends to the two-dimensional limit

$$\varphi(z_e, z_h, \rho) = \sqrt{2/\pi}(4/Wa_B)\cos(\pi z_e W) \times \cos(\pi z_h/W)\exp(-2\rho/a_B),$$

where $W$ is width of the QW.

The exciton binding energy can be obtained as follows [16,22]:

$$E_b = E_{e1} + E_{h1} - \langle\varphi|H_{diag}|\varphi\rangle = E_{e1} + E_{h1} - E_x, \quad (2)$$

where $E_{e1}$ is electron quantization level relative to the bottom of the conduction band in the QW, $E_{h1}$ is hole quantization level relative to the top of the valence band in the QW, $E_x$ is position shift of the level of the exciton state relative to the band gap in the QW. The magnitude of radiation broadening, according to [16,22], is determined as follows:

$$\hbar\Gamma_0 = 2\pi\mathbf{q}/\varepsilon(e|\mathbf{p}_{cv}|/m_0\omega_0)^2 \left|\int_{-\infty}^{\infty}\Phi(z)\exp(i\mathbf{q}z)dz\right|^2, \quad (3)$$

where $\mathbf{q}$ is photon wave vector; $|\mathbf{p}_{cv}|$ is matrix element of the interband transition; $\Phi(z) \equiv \equiv \varphi(z_e = z_h = z, \rho = 0)$ — cross section of the exciton wave function for the same electron and hole coordinates.

## 4. Potential of the QW

### 4.1. Effect of mechanical stresses

The mismatch between the lattice constants of $In_xGa_{1-x}As$ and GaAs results in the mechanical stress of the solid solution layer. In this case, the band discontinuity is determined both by the concentration of the solid solution and by the stress, which affects the band shift and the magnitude of the band splitting of light and heavy holes [9–14,17]. The change in the band gap due to hydrostatic compression for a heterostructure grown along the (001) direction is given by the following expression:

$$\delta E^H = a(x)\big(2 - \lambda^{001}(x)\big)\varepsilon(x),$$

where $\varepsilon(x) = \big(a_0(x) - a_0\big)/a_0$ is strain due to a change in the lattice constant $a_0$ in the solid solution layer; $a(x) = a_v(x) + a_c(x)$ is hydrostatic deformation potential; $\lambda^{001}(x) = 2c_{12}(x)/c_{11}(x)$, where $c_{11}(x)$ and $c_{12}(x)$ are elastic stiffness constants. The shift of the conduction band edge and the valence band edge in a solid solution under the action of hydrostatic compression (tension) can be specified either by a constant coefficient $Q^H$, then $a_c(x) = a(x)Q^H/(1 + Q^H)$, $a_v(x) = a(x)/(1 + Q^H)$, or by using interpolation between $a_v$ and $a_c$ for GaAs and InAs.

Splitting of the valence bands of light and heavy holes due to compression along the (001) direction is:

$$\delta E^S = -b(x)\big(1 + \lambda^{001}(x)\big)\varepsilon(x),$$

where $b(x)$ is shear deformation potential.

Taking into account the presence of stresses, the position of the edge of the conduction band edge and the valence bands of light and heavy holes is given by the following expressions:

$$E_c = \frac{Q}{1+Q}E_g^{\mathrm{InGaAs}} + a_c(x)\delta E^H,$$

$$E_v(hh) = \frac{1}{1+Q}E_g^{\mathrm{InGaAs}} + a_v(x)\delta E^H - \delta E^S,$$

$$E_v(lh) = \frac{1}{1+Q}E_g^{\mathrm{InGaAs}} + a_v(x)\delta E^H - [\Delta_{SO} - \delta E^S]/2 + 1/2\sqrt{\Delta_{SO}^2 + 2\Delta_{SO}\delta E^S + 9(\delta E^S)^2},$$

where $\Delta_{SO}$ is magnitude of the spin-orbit splitting; $Q$ is ratio of conduction and valence band discontinuities in the QW with the unstrained layer in the $In_xGa_{1-x}As$ solid solution (Figure 2, *a*).

A potential barrier is formed for the light hole in the given range of indium concentrations. In this case, the bound state is formed due to the Coulomb potential of the electron in the QW and the light hole [14,18].

### 4.2. The segregation effect

For $GaAs/In_xGa_{1-x}As$ structures, the concentration profile in the solid solution layer is determined by the process of segregation of In atoms. According to the model of [16], it can be described by the following formula:

$$f(z) = \begin{cases}[1 - \exp(-z/\lambda_d)], & 0 < z < L^{QW},\\ [1 - \exp(-z/\lambda_d)]\exp\big(-(z - L)/\lambda_d\big), & z > L^{QW}.\end{cases}$$

Here $L^{QW}$ is QW width (thickness of the layer grown with the shutter open); $\lambda_D$ is parameter describing the effective segregation length (Figure 2, *b*), $\lambda_D = 5.79$ nm at $T = 520°C$ [16].

### 4.3. Effective masses of light and heavy holes

An essential parameter that determines the exciton binding energy is the effective mass of light and heavy holes in the QW plane. The effective mass of holes in the QW is determined by the concentration of the solid solution, the degree of localization of the wave function of the light and heavy holes in the QW, and the magnitude of the stress in the localizing layer [11,12,17]. In a QW with infinite barriers, the effective mass of light and heavy holes in a plane parallel to the heterointerface is given by the following expression: $m_{xy} = 1/(\gamma_1 \pm \gamma_2)$, where $\gamma_1, \gamma_2$ are Luttinger parameters.

For a narrow QW, the degree of delocalization of wave functions is high, and, according to the theoretical calculation [17], the effective mass of a light hole in the plane of the well, $m_{xy}$, tends to $m_{lh}$, and the effective mass of a heavy hole tends to $\sqrt{m_{hh}m_{lh}}$, where $m_i = 1/(\gamma_1 \mp 2\gamma_2)$ is the value for the heavy (upper sign) and light (lower sign) holes. It should be noted that the change in the effective mass of light and heavy holes in narrow quantum wells of $In_xGa_{1-x}As/GaAs$ with a finite depth relative to the mass $m_{xy} = 1/(\gamma_1 \pm \gamma_2)$ obtained for quantum wells with infinite barriers was also observed experimentally [18–21].

## 5. Microscopic calculation

A feature of modeling the exciton spectrum of a narrow QW is the need to take into account the strong penetration of the wave functions of QW-localized excitons into the barriers. Therefore, a separate task was the choice of the width of the integration region ($W_{int}$). In this context, the exciton spectrum was modeled with varying the width of the integration region.

In order to identify excitonic states localized in the QW, a comparison was made of the spectrum of exciton states of the region containing the QW (the heterostructure with a QW) and the region not containing the QW (the homogeneous layer). Microscopic calculations were carried out for 10 heavy hole excitonic states and 10 light hole excitonic states.

A comparison of the spectra of heavy hole and light hole excitonic states for the heterostructure with a QW and the homogeneous layer, obtained using microscopic calculations, is shown in Figure 3. The states of the exciton spectrum of the heterostructure with a QW can be divided into two types. Energy position and magnitude of radiation broadening of states with $n(hh) = 1$ and $n(hh) = 2$ for a heavy hole exciton (Figure 3, *a*–*b*), as well as with $n(lh) = 1$ for a light hole exciton (Figure 3, *c*–*d*), are determined by the parameters of the narrow QW potential and do not depend on $W_{int}$ with $W_{int} > 300$ nm. In this case, the energy interval between the $n(hh) = 1$ and $n(hh) = 2$ states is determined by the ratio of band discontinuities in the QW. Thus, states with $n(hh) = 1$ and $n(hh) = 2$ for the heavy hole exciton and with $n(lh) = 1$ for the light hole exciton can be referred to as QW-localized states.

The spectrum of states with $n > 2$ for the heavy hole exciton in the case of the heterostructure with a QW and in the case of a homogeneous layer are well consistent with each other, subject to the following replacement (shift): $n \to n - 1$ (Figure 3, *a*). For the light hole exciton, the positions of energy levels with $n > 1$ for the heterostructure with a QW coincide well with the dependence on $n$ for a homogeneous layer (Figure 3, *c*). Such states will be referred to as delocalized exciton states. Their spectrum, as well as the spectrum of an exciton in the homogeneous layer with a thickness of $W_{int}$, can be represented as points on the dispersion of a mechanical exciton in a bulk material [27]. The parameters of the spectrum of delocalized states are weakly sensitive to the potential of a narrow QW. Microscopic calculations show that the magnitude of the radiation broadening of exciton resonances with $1 < n(hh) < 4$ for the homogeneous layer and for the heterostructure with a QW with $3 < n(hh) < 6$ exceeds the energy gap between them. This is indicative of the formation of a continuous spectrum region.

As mentioned above, the methods used for isolated excitonic states in this case cannot provide a correct description of the contribution of excitonic states to the optical spectra. At the same time, for the homogeneous layer with a width of $W > 12a_B^{exc}$, the contribution of excitonic states to the optical spectra can be modeled within the framework of the dielectric constant formalism taking into account spatial dispersion [27,28]. The features of optical spectra in the region of excitonic resonances can be considered from the point of view of the interference of polariton waves on a layer of finite thickness, both in the case of non-degenerate bands [27] and in the case of degenerate bands [29].

The most direct information about the energy position of excitonic states can be obtained from the absorption spectrum. The absorption spectrum for a layer of finite thickness can be calculated from the reflection and transmission spectra [30]. In the region where the quasi-continuous exciton spectrum is located, the absorption coefficient is determined primarily by the imaginary part of the refraction indices of the exciton and photon-like modes [31]. The inset in Figure 3, *b* shows the spectrum of absorption coefficient calculated in the formalism of dielectric constant taking into account spatial dispersion for a layer with a thickness of 361.6 nm, a non-radiation broadening of $\hbar\Gamma_{NR} = 7.5\,\mu$eV, taking into account the contribution of the heavy hole exciton. The position of the long-wavelength edge of the quasi-continuous spectrum is consistent with the microscopic calculation. In the interval from 1514.73 to 1515.4 meV, a band of a quasi-continuous spectrum of exciton states is observed. Individual maxima located at higher energies correspond to the levels of size quantization of the heavy hole exciton in a layer with a thickness of $W_{int}$. The maxima of the calculated absorption coefficient and the positions of exciton resonances obtained from the microscopic calculation are well consistent with each other (Figure 3, *b* inset).

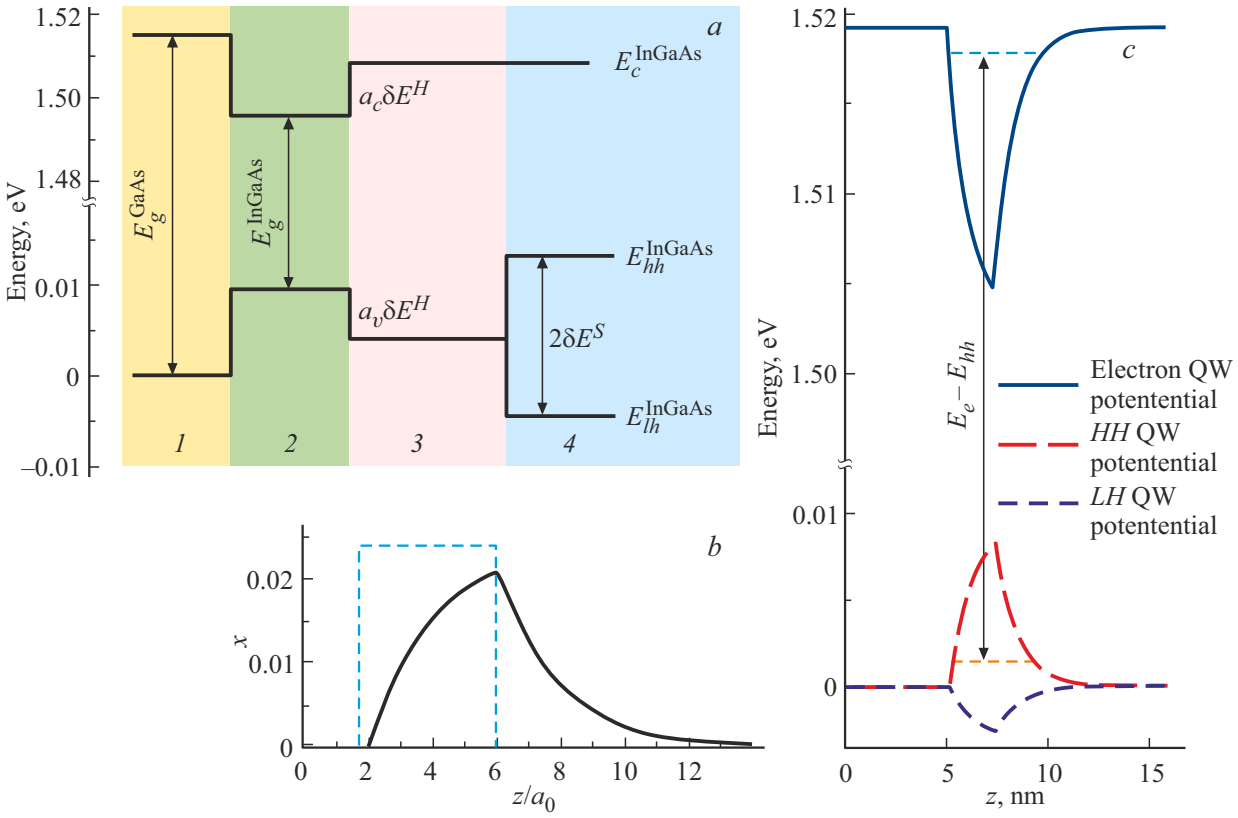


**Figure 2.** *a* — position of the edges of the conduction band and light and heavy hole valence bands: *1* — in gallium arsenide; *2* — in $In_xGa_{1-x}As$ unstrained solid solution; *3* — in $In_xGa_{1-x}As$ solid solution taking into account hydrostatic stress; *4* — in $In_xGa_{1-x}As$ solid solution taking into account hydrostatic and uniaxial stress. *b* — change in the concentration of In atoms depending on the layer number ($z/a_0$): without taking into account the segregation (dashed line) under the effect of segregation (solid line); *c* — model of QW potential: solid line — electron QW, dashed line — heavy hole QW, dotted line — light hole barrier. The arrow shows the transition between the size quantization levels of electron and heavy hole.

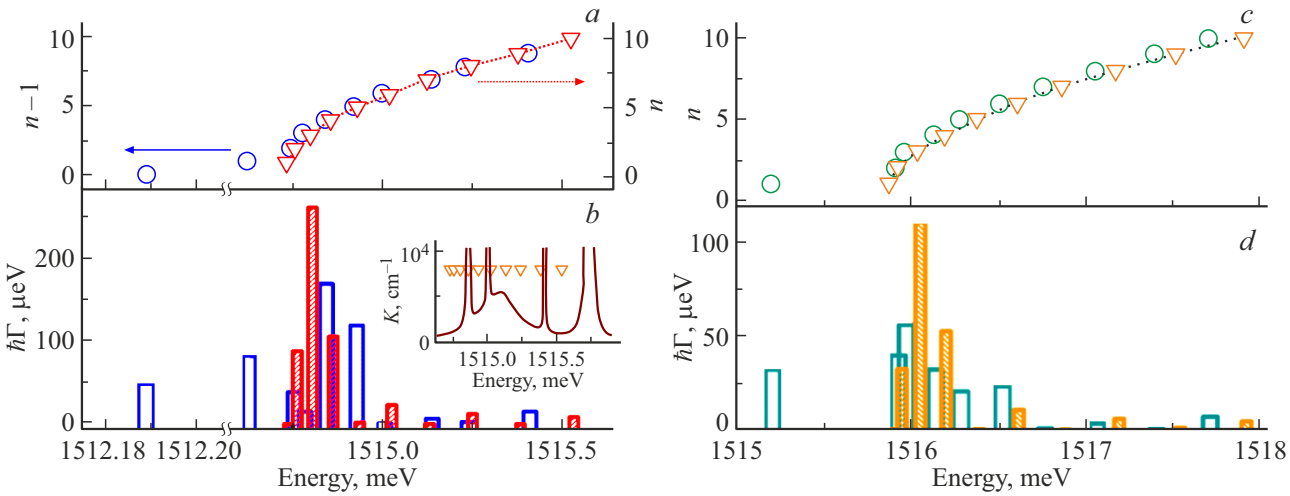


**Figure 3.** Spectrum of heavy and light hole excitons, obtained within the framework of microscopic calculations. For the heavy hole exciton heavy and light hole excitons: (*a*) — dependencies of the state number on its energy; circles — heterostructure with QW, triangles — homogeneous layer; (*b*) — dependence of radiation broadening on energy: white bars — heterostructure with QW, shaded bars — homogeneous layer. (*c*) and (*d*) — the same for the light hole exciton. Inset: solid line — absorption coefficient spectrum, triangles — exciton resonance energies obtained in the microscopic calculation.

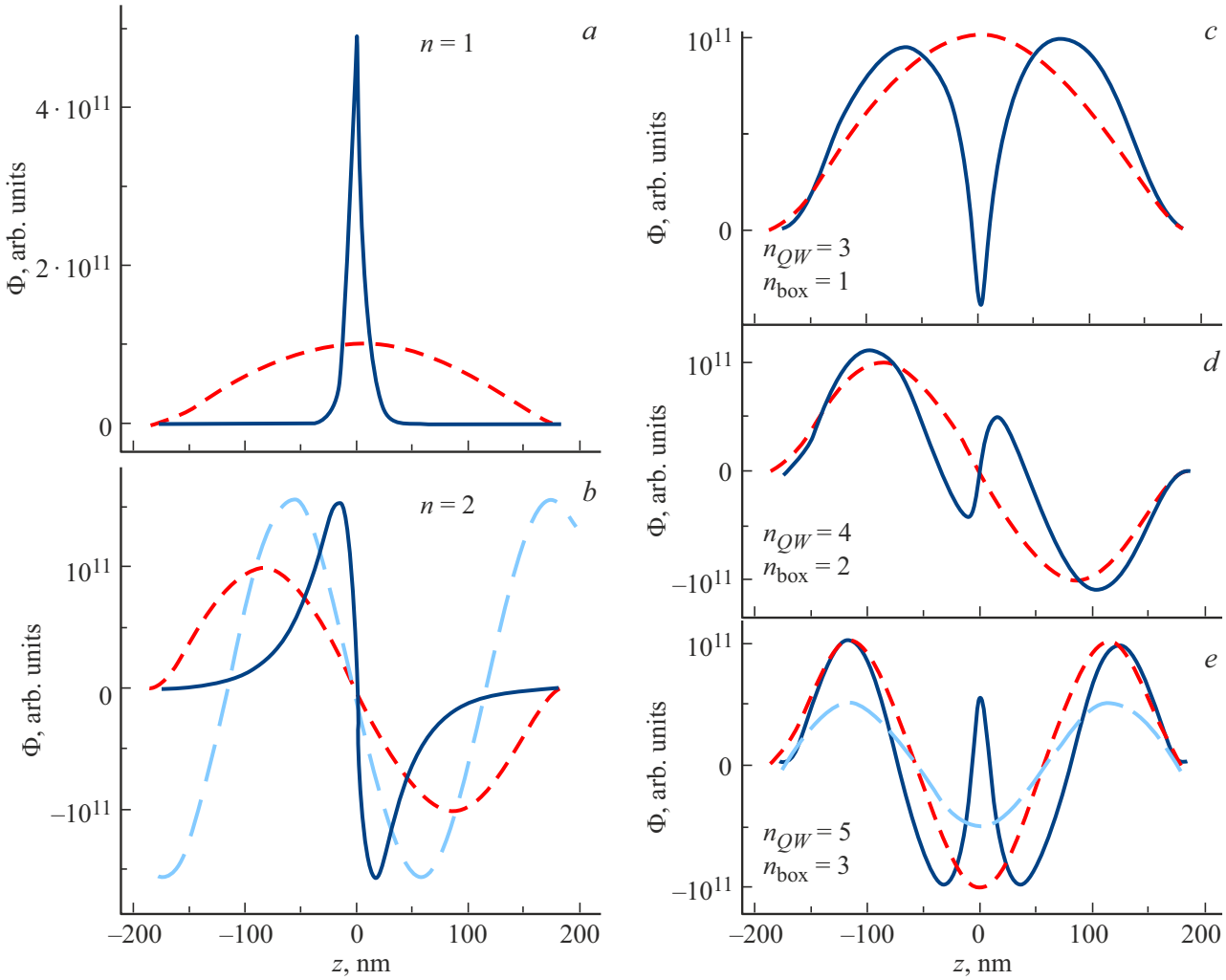


**Figure 4.** $\Phi(z)$ functions of the first 5 exciton resonances for the heterostructure with a QW (solid lines) and without a QW (dashed lines), calculated with the parameters of the heavy hole exciton. The state numbers, $n_{\text{QW}}$ (for heterostructure with a QW) and $n_{\text{box}}$ (for a homogeneous layer), are indicated in the figure. The spatial distribution of the electric field strength of an electromagnetic wave ($\lambda = 818$ nm) in a medium with $\varepsilon = 12.53$ is shown by long dashed lines.

The spatial distribution of the $\Phi(z)$ function also confirms the division of excitonic states in a layer with a QW into two types: localized in the QW region and delocalized ones. The form of the $\Phi(z)$ function for heavy and light hole excitons in a homogeneous layer expectedly corresponds to the form of the corresponding function in the problem of quantizing the center of mass of an exciton in an infinitely deep QW with a width of $W_{int}$.

A comparison of $\Phi(z)$ functions for the first two excitonic states in the heterostructure with a QW and the homogeneous layer confirms the localization of excitonic states with $n(hh) = 1$ and $n(hh) = 2$ for heavy hole excitons (Figure 4, *a, b*) and with $n(lh) = 1$ for the light hole exciton (Figure 5, *a*) by the QW potential considered in this study. The $\Phi(z)$ function for the heterostructure with a QW of the state with $n(hh) = 1$ is most strongly localized in the QW region (Figure 4, *a*). The change in the form of the $\Phi(z)$ function of the heterostructure with a quantum well for the $n(hh) = 2$ state relative to $\Phi(z)$ $n(hh) = 2$ for the homogeneous layer also indicates a significant effect of the localizing potential of a narrow QW on this state (Figure 4, *b*).

Let us compare the $\Phi(z)$ functions of excitonic states for the homogeneous layer and delocalized excitonic states of the heterostructure with a QW. In Figure 4, *c*–*e* the $\Phi(z)$ functions are compared for the first three states in the homogeneous layer ($n_{box} = 1, 2, 3$) and for the first three delocalized states in the heterostructure with a QW ($n_{QW} = 3, 4, 5$). For the delocalized exciton states in the heterostructure with a QW, the $\Phi(z)$ functions occupy the entire region of integration over $z$, just as for the homogeneous layer. In the barrier region, the $\Phi(z)$ of the heterostructure with a QW corresponds well to the behavior of $\Phi(z)$ for the homogeneous layer. The effect of the QW on the delocalized states of the heavy hole exciton

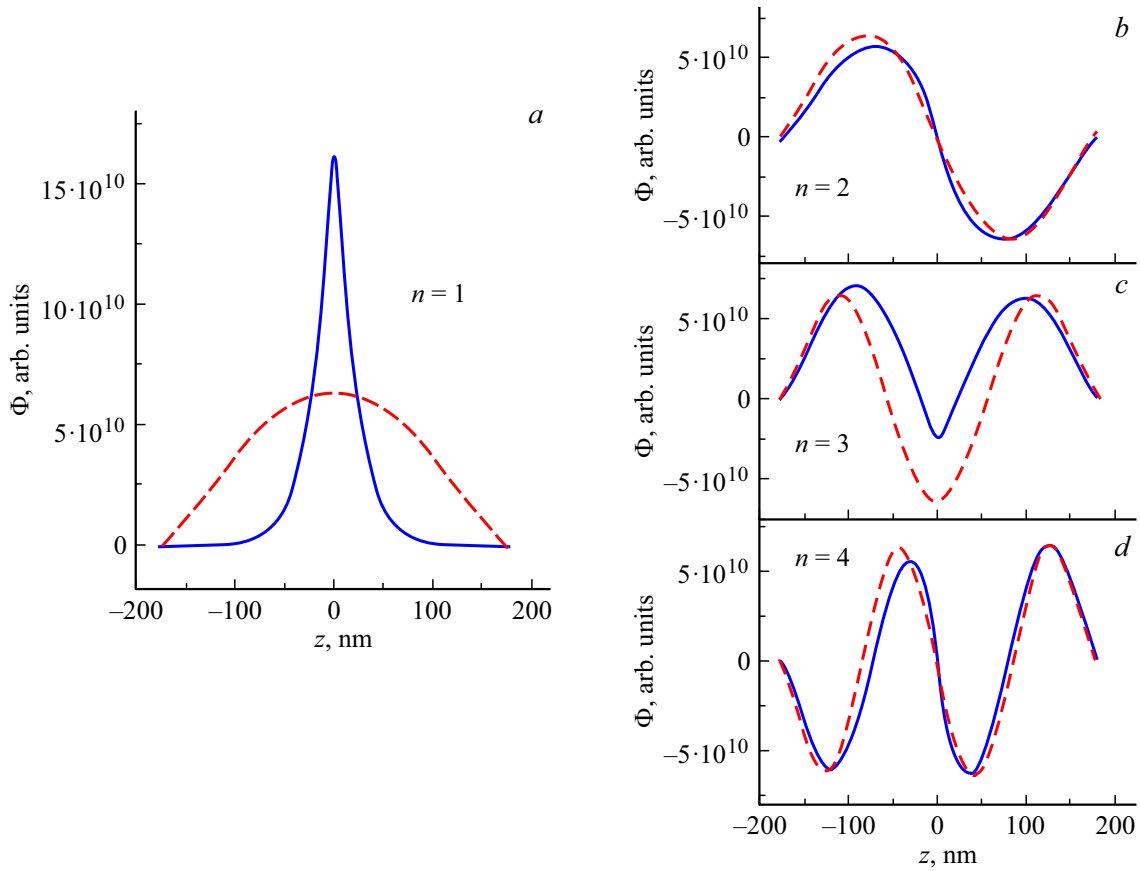


**Figure 5.** $\Phi(z)$ functions of the first 4 exciton resonances for the heterostructure with a QW (solid lines) and the homogeneous layer (dashed lines), calculated with the parameters of the light hole exciton.

is manifested in the redistribution of the $\Phi(z)$ function near the QW (Figure 4, $c$–$e$).

For the light hole exciton, the $\Phi(z)$ functions of even states of the heterostructure with a QW and the homogeneous layer basically coincide (Figure 5, $b$, $d$). For odd delocalized states, a decrease in the probability amplitude of the $\Phi(z)$ function near the QW is observed, compared to the distribution of the probability amplitude of this function for the homogeneous layer (Figure 6, $c$). This can be associated with the repulsive effect of the barrier formed by the layer of $In_xGa_{1-x}As$ ($x < 0.2$) for a light hole.

It is noteworthy that within the framework of microscopic calculations, the magnitude of the radiation broadening of the exciton state $n(hh) = 1$ is less than that of $n(hh) = 2$. This is explained by the difference in the overlap integrals of the $\Phi(z)$ function and the electric field strength of a light wave in GaAs with a wave vector $\mathbf{q}$ corresponding to a wavelength of 818 nm. The $\Phi(z)$ function for $n(hh) = 1$ is highly localized, and the light wave field strength when calculating the $\hbar\Gamma_0$ can be considered a constant value. In this case, the magnitude of radiation broadening coincides well with the magnitude of the oscillator strength [16,22,24,25]. The $\Phi(z)$ function of the $n(hh) = 2$ state occupies a wider area. A comparison of the $\Phi(z)$ $n(hh) = 2$ function and the light wave amplitude proportional to $\sin(\mathbf{qr})$ allows concluding the greater integral (3) for the $n(hh) = 2$ state than that for the $n(hh) = 1$ state.

Within the chosen model, the long-wavelength part of the exciton spectrum is formed by the QW-localized heavy hole exciton. In this case, the $n(hh) = 1$ and $n(hh) = 2$ states are below the exciton energy in GaAs (1515 meV). These states can be referred to the $X1$ and $X2$ resonances in the experimental reflection spectrum. In the higher energy region there is the band of the quasi-continuous spectrum and the levels of size quantization of the exciton in the heterostructure with a QW. The spectrum of states of light hole excitons, due to the splitting of the valence band under the effect of stress, is located above the energy of 1515 meV.

## 6. Determination of localizing potential parameters and reflection spectrum analysis

To select the parameters of the localizing potential, a region with a width of $W_{int} = 640a_0 = 361.6$ nm was chosen. The best agreement with the experimental position of the excitonic resonances $X1$ and $X2$ with the resonant frequencies of the $n(hh) = 1$ and $n(hh) = 2$ states

obtained by microscopic calculation is achieved with the following parameters specifying the potential of a narrow QW. Indium concentration: $x = 0.022$, QW width: $L^{QW1} = 4a_0 = 2.26$ nm. When modeling the QW potential, the following values of constitutive parameters were used:

$$\varepsilon = 12.53 + 1.08x, \quad a_v = -1.16 + 0.16x,$$

$$a_c = -7.17 + 2.09x, \quad b = -1.90 + 0.35x,$$

$$c_{11}(x) = 12.25 - 3.921x, \quad c_{12}(x) = 5.71 - 1.184x,$$

given in [12,14], as well as $Q = 85:15$ [10,13,15]. The $\gamma_1, \gamma_2$ parameters were calculated in accordance with the data given in [16]. This yielded following relationship between the discontinuities of the conduction bands and the heavy hole valence band $E_c : E_v = 64:36$. Thus, the experimental data are well described by the values of the ab initio calculated constitutive parameters on the basis of the theoretical approach outlined in [10]. This approach represents the interface region as a crystal consisting of neutral spherical atoms, the pseudopotentials for which are calculated ab initio, and uses the local density approximation to calculate the band structure. It makes it possible to reduce the positions of the band edges of substances forming a heterojunction to an absolute energy scale and take into account their changes under the action of elastic stresses. This approach should give good results for a pseudomorphic layer, which a narrow QW in a high-quality heterostructure is.

The final model of the localizing potential is shown in Figure 2, *c*. It should be noted that when calculating the parameters of excitonic states for the heavy hole exciton, the band gap was determined as the energy interval between the minimum of the conduction electron potential (Figure 2, *c*, solid line) and the maximum of the heavy hole potential (Figure 2, *c*, long-dashed line). And when calculating the parameters of excitonic states for the light hole exciton, the band gap was determined as the energy interval between the minimum of the conduction electron potential (Figure 2, *c*, solid line) and the maximum of the light hole potential (Figure 2, *c*, short-dashed line). The parameters of excitonic states localized in the QW region, obtained using microscopic calculations, are given in Table 2.

With known parameters of excitonic states and the quantum well potential, it is possible to analyze the nature of the observed excitonic transitions. Let us estimate the exciton binding energy by substituting into expression (2) the parameters obtained from the microscopic calculation (Table 2) and the positions of the exciton resonances $X1$ and $X2$, obtained directly from the experimental data (see Table 1).

$E_{e1}$ and $E_{h1}$ can be determined by solving the one-dimensional problem using microscopic modeling for the final model of the localizing potential. The electron level in the QW is $E_{e1} = 14.30$ meV, and for the heavy hole it is $E_{h1} = 7.42$ meV.

**Table 2.** Parameters of excitonic states localized in the QW region, obtained using microscopic calculations

| Resonance | $n(hh) = 1$ | $n(hh) = 2$ | $n(lh) = 1$ |
|---|---|---|---|
| $\hbar\omega_0$, meV | 1512.19 | 1514.63 | 1515.19 |
| $\hbar\Gamma_0$, $\mu$eV | 51 | 79 | 11 |
| $E_x$, meV | 16.17 | 18.61 | 8.37 |

With $E_{e1}$ and $E_{h1}$, it is possible to estimate the energy of possible interband transitions in the heterostructure with the QW (Figure 6, *a*) and estimate the exciton binding energy for each of them, knowing the positions of exciton resonances $X1$ and $X2$. For a spatially direct transition: $E_{e1} - E_{h1} E_b^{X1} = 5.55$ meV, $E_b^{X2} = 3.11$ meV; for spatially indirect transitions: $E_c - E_{h1} E_b^{X1} = 6.15$ meV; $E_b^{X2} = 3.72$ meV; for the transition $E_{v(hh)} - E_{e1} E_b^{X1} = 6.41$ meV, $E_b^{X2} = 3.97$ meV.

The exciton binding energy calculated using the microscopic calculation data for $n(hh) = 1$ will be $E_b^{n1} = 5.55$ meV, for $n(hh) = 2$ it will be $E_b^{n2} = 3.11$ meV. Thus, the quantities $E_b^{n1}$ and $E_b^{n2}$ coincide with the exciton binding energies for a spatially direct transition. It can be concluded that the $X1$ and $X2$ resonances observed in the reflectance spectrum are contributions from the ground state and the first excited state of the heavy hole exciton from the spatially direct transition to the QW. The spectrum of QW-localized heavy hole excitonic states is represented by 2 states and is not described by the model for a hydrogen-like system with a fractional dimension [32].

The same estimate can be made for the light hole exciton. In this case, the position of the exciton state $n(lh) = 1$ can be determined only from the microscopic calculation (see Table 2). Exciton binding energy obtained using expression (2) and the value of $E_x$ obtained from the microscopic calculation: $E_b^{LH} = 3.38$ meV. Using the values of the $E_{e1}$ parameter, it can be shown that for the $E_{v(lh)}^{\mathrm{InGaAs}} - E_{e1}$ spatially direct transition the binding energy must be at least 5.93 meV. At the same time, for the $E_{v(lh)}^{\mathrm{GaAs}} - E_{e1}$ spatially indirect transition the binding energy can be estimated as $E_b^{LH} = 3.41$ meV. Consequently, the excitonic state $n(lh) = 1$ belongs to a spatially indirect transition. This is also confirmed by the data on the nature of the light hole exciton in the $In_xGa_{1-x}As/GaAs$ quantum well with $x < 0.2$, presented in [14,18].

Figure 6, *a* shows a comparison of the experimental reflectance spectrum with the calculation within dielectric response model (1) in the energy range from 1512 to 1519.5 meV using parameters obtained within the microscopic calculation. The parameters of the $X1$ resonance obtained from the microscopic calculation and the dielectric response model are in good agreement with each other. For the $X2$ resonance, the magnitude of the radiation broadening obtained from the microscopic calculation differs from that obtained using the dielectric response model.

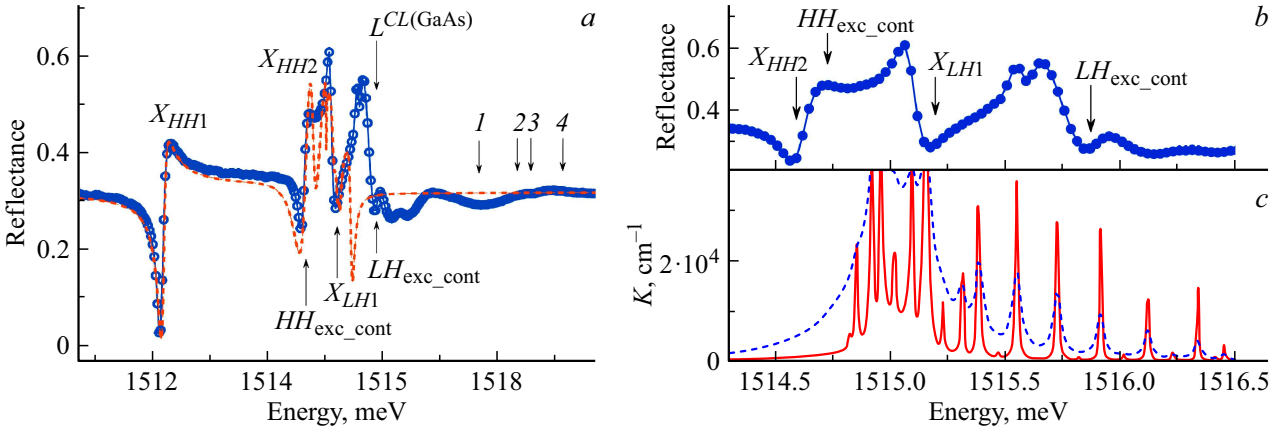


**Figure 6.** *a* — experimental reflectance spectrum of the P552 sample (circles); model reflectance spectrum calculated using expression (3) with parameters obtained from microscopic calculations (dashed line); *b* — experimental reflectance spectrum of the P552 sample (circles); *c* — spectrum of the absorption coefficient calculated in the dielectric constant formalism taking into account spatial dispersion for a region with a width of 1232 nm: $\hbar\Gamma_{NR} = 7.5\,\mu$eV — solid line, $\hbar\Gamma_{NR} = 37.5\,\mu$eV — dotted line. The arrows show: $HH_{exc\_cont}$ — position of the long-wave edge of the quasi-continuous spectrum of the heavy hole exciton; $LH_{exc\_cont}$ — position of the long-wavelength edge of the quasi-continuous spectrum of the light hole exciton; $L^{CL(GaAs)}$ — position of the first exciton resonance in the cap layer of the heterostructure (microscopic calculation data); *1* — $E_{e1}-E_{h1}$ transition; *2* — $E_c^{GaAs}-E_{h1}$ transition; *3* — $E_{e1}-E_v^{GaAs}$ transition; *4* — $E_c^{GaAs}-E_v^{GaAs}$ transition.

This is explained by the proximity of this resonance to the region of the quasi-continuous spectrum. In this case, the amplitude of the state's contribution to the reflectance spectrum is determined by the mutual influence of nearby resonances [23–25]. The position of the $X_{LH1}$ isolated light hole excitonic resonance and the beginning of the quasi-continuous spectrum of light hole excitonic states $LH_{exc\_cont}$ are shown with arrows.

The spectral positions of the $X3-X5$ features do not correspond to the resonant frequencies of the QW-localized excitonic states obtained from the microscopic calculation. On the other hand, the analysis showed that a narrow QW does not introduce a strong disturbance into the spectrum of excitonic states above the quantum well. Therefore, the contribution of the spectrum of delocalized excitonic states to the optical properties of the heterostructure can be assessed using the absorption spectrum calculated in the formalism of dielectric constant with a spatial dispersion. The calculation was carried out for a homogeneous layer with a thickness corresponding to the sum of the width of a narrow QW and the barriers surrounding it: $L^{BfL} + L^{QW1} + L^{Br} = 1232$ nm (Figure 6, *c*) using two values of $\Gamma_{NR}$. The small value of $\hbar\Gamma_{NR} = 7.5\,\mu$eV (Figure 6, *c*, solid line) allows visualizing the structure of the polariton spectrum above the energy of 1515 meV. The second value of $\hbar\Gamma_{NR} = 37.5\,\mu$eV was chosen close to the values of $X3-X5$ resonances obtained from the analysis of the experimental spectrum (Figure 6, *c*, dashed line). In the absorption spectrum, an interval can be distinguished corresponding to the quasi-continuous exciton spectrum (from 1514.73 to 1515.5 meV); in the higher energy region there are the maxima determined by quantization of the center of mass of the exciton in the $L^{BfL} + L^{QW1} + L^{Br}$ layer. It can be seen that in the region of $X3-X5$ resonances, the features of the calculated absorption spectrum retain a significant amplitude even when the value of the non-radiation broadening increases to a value of $\hbar\Gamma_{NR} = 37.5\,\mu$eV. The good agreement between the features of the calculated absorption spectrum and the reflectance spectrum (Figure 6, *b, c*) allows concluding that the polariton interference on the $L^{BfL} + L^{QW1} + L^{Br}$ heterostructure layer makes a significant contribution to the formation of the reflectance spectrum of a given sample in the energy range above the level of 1515 meV.

## 7. Conclusion

Thus, the contribution of the narrow QW to the exciton spectrum of the $In_xGa_{1-x}As/GaAs$ heterostructure has been analyzed, isolated excitonic resonances have been identified, and their parameters have been determined. It has been established that two excitonic resonances located below the free exciton energy in GaAs are formed by the heavy hole exciton; the contribution of the light hole exciton localized by the narrow QW is above the level of 1515 meV. It is shown that for modeling the exciton spectrum of heterostructures with narrow QWs and a low concentration of the narrow-bandgap component, the band discontinuity ratio of $E_c : E_v = 64 : 36$ is suitable, which is obtained using theoretical values of constitutive parameters calculated within the the model-solid theory [10].

### Funding

The authors (I.V. Ignatiev and A.V. Mikhailov) thank the Russian Science Foundation for the financial support under grant No. 19-72-20039-P during the experimental research.

The authors (N.R. Grigorieva and E.S. Khramtsov) thank the St. Petersburg State University for the financial support under grants No. 106788664 and No. 9427165 during the theoretical calculations. The authors thank the „Nanoconstruction of Photoactive Materials (Nanophotonics)“ Resource Center of the St. Petersburg State University for the grown samples.

### Conflict of interest

The authors declare that they have no conflict of interest.

## References

[1] J.J. Coleman, P.K. York, K.J. Beernink. Laser Diode Technology and Applications **II**, *1219*, 32 (1990).
[2] P.V. Bulaev, V.A. Kapitonov, A.V. Lutetsky, A.A. Marmalyuk, D.B. Nikitin, D.N. Nikolayev, A.A. Padalitsa, N.A. Pikhtin, A.D. Bondarev, I.D. Zalevsky, I.S. Tarasov. FTP, **36**, 1144 (2002). (in Russian).
[3] Kwang Woong Kim, Jin Dong Song, Won Jun Choi, Jung I Lee. J. Korean Phys. Soc. **49**, 1169 (2006).
[4] A. Stöhr, O. Humbach, S. Zumkley, G. Wingen, G. David, D. Jäger, B. Bollig, E.C. Larkins J.D. Ralston. Opt. Quantum Electron. **25**, S865 (1993).
[5] S.W. Lee, K.U. Chu, S.W. Kim, S. Park, O'D. Kwon, K.W. Goossen, S.S. Pei. Appl. Phys. Lett. **64**, 3065 (1994).
[6] L. Tinkler, P.M. Walker, E. Clarke, D.N. Krizhanovskii, F. Bastiman, M. Durska, M.S. Skolnick. Appl. Phys. Lett. **106**, 021109 (2015).
[7] D. Ballarini1, M. De Giorgi, E. Cancellieri, R. Houdré, E. Giacobino, R. Cingolani, A. Bramati, G. Gigli, D. Sanvitto1. Nature Commun **4**, 1778 (2013).
[8] T. Kuriakose, P.M. Walker, T. Dowling, O. Kyriienko, I.A. Shelykh, P. St-Jean. Nature Photon. **16**, *8*, 566 (2022).
[9] G.L. Bir, G.E. Pikus. Simmetriya i deformacionnye effekty v poluprovodnikakh, Nauka, M., (1972) 584 s. (in Russian).
[10] Chris G. Van de Walle. Phys Rev B **39**, *3*, 1871 (1989).
[11] D.J. Arent, K. Deneffe, C. Van Hoof, J. De Boeck, G. Borghs. J. Appl. Phys. **66**, 1739 (1989).
[12] I. Vurgaftman, J.R. Meyer, L.R. Ram-Mohan. J. Appl. Phys. **89**, 5815 (2001).
[13] K.W. Böer, U.W. Pohl. Semiconductor Physics. Springer Cham (2018). 1299 p.
[14] A.V. Kavokin, S.I. Kokhanovsky, A.I. Nesvizhsky, M.E. Sasin, R.P. Seisyan, V.M. Ustinov, A.Yu. Egorov, A.E. Zhukov, S.V. Gupalov. FTP, **31**, 1109 (1997). (in Russian).
[15] S.V. Poltavtsev, Yu.P. Efimov, Yu.K. Dolgikh, S.A. Eliseev, V.V. Petrov, V.V. Ovsyankin. Solid State Commun. **199**, 4751 (2014).
[16] E.S. Khramtsov, P.A. Belov, P.S. Grigoryev, I.V. Ignatiev, S.Yu. Verbin, Yu.P. Efimov, S.A. Eliseev, V.A. Lovtcius, V.V. Petrov, S.L. Yakovlev. J. Appl. Phys. **119**, 184301 (2016).
[17] L.G. Grechikov, A.V. Subashiev. FTP **27**, 446 (1993). (in Russian).
[18] R.P. Seisyan, A.V. Kavokin, Kh. Moumanis, M.E. Sasin. FTT **59**, 1133 (2017). (in Russian).
[19] Kyu-Seok Lee, El-Hang Lee. ETRI J. **17**, 13 (1996).
[20] Kyu-Seok Leea, Chae-Deok Lee, Yongmin Kim, Sam Kyu Noh. Solid State Commun. **128**, 177 (2003).
[21] R. Samti, F. Raouafi, M. Chaouach, M. Maaref, A. Sakri, J. Even, J.-M. Gerard, J.-M. Jancu. Appl. Phys. Lett. **101**, 012105 (2012).
[22] E.L. Ivchenko. Optical Spectroscopy of Semiconductor Nanostructures. Alpha Science, Harrow (2005). 427 p.
[23] M.M Voronov, E.L. Ivchenko, V.A. Kosobukin, A.N. Poddubny. FTT **49**, *9*, 1709 (2007). (in Russian).
[24] E.S. Khramtsov, P.S. Grigoryev, D.K. Loginov, I.V. Ignatiev, Yu.P. Efimov, S.A. Eliseev, P.Yu. Shapochkin, E.L. Ivchenko, M. Bayer. Phys. Rev. B **99**, 035431 (2019).
[25] M.N. Bataev, M.A. Chukeev, M.M. Sharipova, P.A. Belov, P.S. Grigoryev, E.S. Khramtsov, I.V. Ignatiev, S.A. Eliseev, V.A. Lovtcius, Yu.P. Efimov. Phys. Rev. B **106**, 085407 (2022).
[26] K. Muraki, S. Fukatsu, Y. Shiraki. Appl. Phys. Lett. **61**, 557 (1992).
[27] V.A. Kiselev, B.V. Novikov, A.E. Cherednichenko. Eksitonnaya spektroskopiya pripoverkhnostnoy oblasti poluprovodnikov, Izd-vo S.-Peterburgskogo un-ta, SPb., (2003) 244 s. (in Russian)
[28] R. Del Solo, D'Andrea. Optical Switching in Low-dimensional Systems. Plenum Publishing Corporation (1989). 289 p.
[29] D.K. Loginov, E.V. Ubyivovk, Yu.P. Efimov, V.V. Petrov, S.A. Eliseev, Yu.K. Dolgikh, I.V. Ignatyev, V.P. Kochereshko, A.V. Selkin. FTT **48**, *11*, 1979 (2006). (in Russian).
[30] A.B. Pevtsov, S.A. Permogorov, A.V. Selkin, N.N. Syrbu, A.G. Umanets. FTP **16**, *8*, 1399 (1982). (in Russian).
[31] N.N. Akhmetdiev. ZhETF **79**, 1534 (1980). (in Russian).
[32] Xing-Fei He. Phys Rev B **43**, *3*, 2063 (1991).

*Translated by Y.Alekseev*